J. Appl. Comput. Mech., 6(3) (2020) 493-504
DOI: 10.22055/JACM.2019.29832.1640

ISSN: 2383-4536
jacm.scu.ac.ir

M&MoCS

Shahid Chamran University of Ahvaz

Journal of Applied and Computational Mechanics

Research Paper

A FEM Multiscale Homogenization Procedure using Nanoindentation for High Performance Concrete

Fazilay Abbès[1], Boussad Abbès[2], Rim Benkabou[3], Aïssa Asroun[4]

[1] GRESPI, University of Reims Champagne-Ardenne
UFR SEN, Campus Moulin de la Housse, Reims, 51687, France, Email: fazilay.abbes@univ-reims.fr
[2] GRESPI, University of Reims Champagne-Ardenne
UFR SEN, Campus Moulin de la Housse, Reims, 51687, France, Email: boussad.abbes@univ-reims.fr
[3] LGC, Department of Civil Engineering, Djillali Liabès University
Rue Kadi Benkadi, Sidi-Bel-Abbès, 22000, Algeria, Email: rm.benkabou@univ-sba.dz
[4] LGC, Department of Civil Engineering, Djillali Liabès University
Rue Kadi Benkadi, Sidi-Bel-Abbès, 22000, Algeria, Email: as.asroun@univ-sba.dz

Received June 03 2019; Revised July 27 2019; Accepted for publication July 30 2019.
Corresponding author: Boussad Abbès (boussad.abbes@univ-reims.fr)
© 2020 Published by Shahid Chamran University of Ahvaz
& International Research Center for Mathematics & Mechanics of Complex Systems (M&MoCS)

Abstract. This paper aims to develop a numerical multiscale homogenization method for prediction of elasto-viscoplastic properties of a high performance concrete (HPC). The homogenization procedure is separated into two-levels according to the microstructure of the HPC: the mortar or matrix level and the concrete level. The elasto-viscoplastic behavior of individual microstructural phases of the matrix are identified from nanoindentation data using an inverse identification method. The micromechanical results are then used as input parameters for numerical elasto-viscoplastic homogenization at microscale. The mortar level is analyzed with numerical homogenization by using the finite element simulation to predict the overall elasto-viscoplastic properties of HPC. The results are compared with macroscopic experimental and analytical results from the literature showing a good agreement.

Keywords: Homogenization, Nanoindentation, Finite element simulation, Elasto-viscoplastic model, Multiscale modeling, High performance concrete.

1. Introduction

High performance concretes are heterogeneous cementitious composites representing one of the most used building materials. In order to predict their behavior or optimize the characteristics of these composites materials, models taking into account the microstructure specifications, such as morphology and the constituent's properties should be developed. Cementitious composites are multiscale materials, since they can be treated as homogeneous in the macroscopic level and as heterogeneous in a finer level of observation. A significant interest is observed in the study of the various length scales that govern the mechanics of materials. To identify the relationships that bridge the various scales, several methods have been proposed in the literature [1]. Analytical or mean-field methods were extensively developed to provide predictions of the macroscopic mechanical properties deriving from preliminary computations on a microscopic scale. Among these methods, the most popular ones are: Eshelby's inclusion theory [2], Voigt-Reuss-Hill's bounds [3], Hashin-Strikman bounds [4] and the self-consistent methods [5].

However, when considering the nonlinear behavior, these methods are difficult to apply and numerical methods which allow simultaneous computations on different scales are an alternative [6-8]. The computational homogenization

Published online: September 15 2019

approach was successfully applied to nonlinear analysis of different composite materials [9-13]. The analytical and numerical homogenization approaches have been applied to determine macroscale elastic properties [14-19] and to study the nonlinear behavior such as damage and failure [20-22] of cementitious composites.

Elasto-viscoplastic models are capable of describing age, rate and stress and strain history dependence especially under loading time dependence of concrete. During the last several decades many works have been devoted to the development of plastic and viscoplastic models, in order to better predict the material behavior under combined variable mechanical loading. Tedesco et al. [23] and Tedesco et al. [24] derived a rate-dependent constitutive model for concrete and implemented their model into a general-purpose finite element code. Reinforced concrete structures subjected to impulsive loading were analyzed by Beshara and Virdi [25] using an elasto-viscoplastic constitutive law for the compressive behavior of concrete as and a linear-elastic/strain-softening for the tensile behavior. The behavior of reinforced concrete structures subjected to dynamic loads was analyzed by Cela [26] using an elasto-viscoplastic concrete model. Numerical simulations of missile impact on reinforced concrete were conducted by Shirai et al. [27] using a material model that accounts for the effects of strain rate. Park et al. [28] analyzed the response of concrete and mortar under high-strain-rate impact loading. A micromechanical model was formulated and used, accounting for the two-phase composite microstructure of concrete. The behavior of the two constituent phases in the concrete were modeled by an extended Drucker–Prager model that accounts for pressure-dependence, rate-sensitivity, and strain hardening/softening. Buck et al. [29] studied the load-carrying and energy dissipation capacities of ultra-high performance concrete (UHPC) under dynamic loading in relation to microstructure composition. Cementitious materials are, so the constitutive relation used must be able to capture both aspects of the behavior. In their study, the Drucker–Prager model was used for the cementitious matrix to take into account both pressure-sensitivity and rate-sensitivity.

Our work aims to develop a numerical two-level homogenization method for prediction of elasto-viscoplastic properties of a high performance concrete (HPC) where the microstructural heterogeneities are analyzed with the nanoindentation. The idea is to propose a simple and unique model for all scales to account for the elasto-viscoplastic behavior of HPC and its constituents without loss of generality. Indeed, more complex behavior models may be used without difficulty by adopting the procedure to be described in the following sections.

2. Numerical Models

2.1 Preliminary Assumptions

The high performance concrete as a heterogeneous material is composed of cementitious matrix (based on blended cement and fly-ash), fine and coarse aggregates and porosity. In the mesoscopic simulation of concrete, biphasic [30-32] and triphasic [33-34] numerical models are frequently used.

Triphasic concrete mesoscopic models assume three homogeneous of mortar, interfacial transition zone (ITZ) and coarse aggregates. Interphase between particles and matrix plays a key role in mechanical and thermal properties of composites. Over the past few decades, considerable efforts have been devoted to theoretically predicting the effective moduli of particle-reinforced composites consisting of reinforced particles, interfaces and matrix. It is worth mentioning that Xu and al. recently utilized a general micromechanical framework [35-38] and DEM–FEM simulation [39] to predict the effective elastic [35-37, 39], thermal and transport properties [36, 38] of particle-reinforced composites containing nonspherical particles and interphases. There have been many other homogeneous models formulated to predict the effective physico-mechanical properties of three-phase composites that have been recently summarized by Xu et al. [40]. However, when dealing with the nonlinear behavior, these methods are difficult to apply and numerical methods are an alternative. By considering ITZ phase, one can capture the local phenomena around aggregates but it requires much more effort in the geometry definition and mesh generation especially for 3D simulations because the length scale of ITZ is much smaller than those of mortar and aggregates.

Biphasic concrete mesoscopic models assume two homogeneous phases of mortar and coarse aggregates, each with its own constitutive law. Hence, the mortar or matrix phase should account for all the concrete mesoscopic constituents, i.e. cement paste, aggregates, interfacial transition zones and porosity. The mechanical behavior of the mortar phase is generally determined by using an effective inverse method to determine the parameters of the constitutive model from the tests on concrete samples [32]. It should be highlighted here that the issue is more critical in inelastic studies rather than elastic ones. In the present study, a biphasic concrete mesoscopic model is adopted based on the experimental work of Da Silva et al. [17]. In their experimental work, the indentation grid was squeezed between the large aggregate; therefore, the properties of possible ITZ are naturally included in the nanoindentation data. Also, the very dense matrix itself consists of possibly interconnecting ITZs surrounding the pure phases.

Considering that the main objective of the current study is the prediction of elasto-viscoplastic properties of a high performance concrete, the following assumptions are made:

- The numerical scheme used in this study solves the problem of finding the effective elasto-viscoplastic properties with a periodically repeating microscopically inhomogeneous RVE by using the finite element (FE) method.
- The microstructure of the high performance concrete is represented by means of 2D biphasic (matrix + aggregates) and porosity using an arbitrary microstructural phase morphologies digitized and explicitly considered in the numerical models as shown in Fig. 1.
- The elasto-viscoplastic deformation is modelled as a superposition of elastic, perfectly plastic and creep

deformations at different scales (matrix constituents, homogenized matrix phase and HPC).

• The coarse aggregates are assumed to behave elastically as it is generally accepted ([21], [31-32]).

• The homogenized elasto-viscoplastic model for the matrix phase is determined through an inverse identification procedure of its different constituents based on nanoindentation mechanical tests.

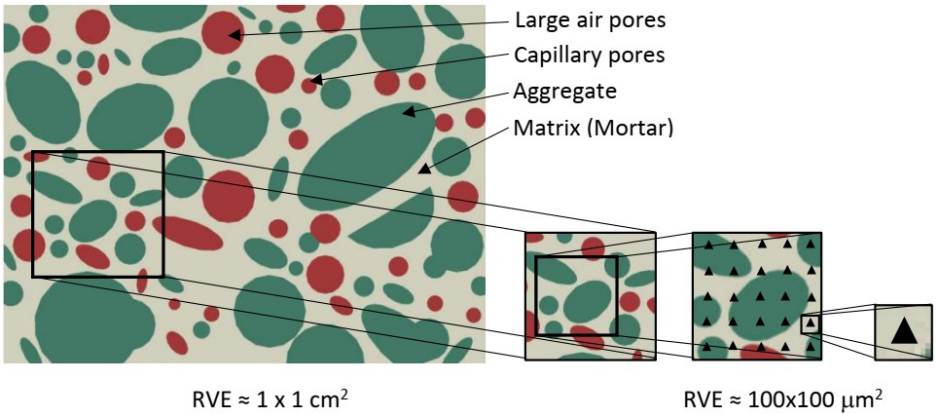

Fig. 1. Representation of the multiscale modeling of high performance concrete.

2.2 Material Behavior

Nonlinear behavior of real material originates both from plastic and viscous internal dissipation of energy. In the theory proposed for rate dependent behavior of plastic materials, Perzyna [41] assumed that the viscous properties of the material become manifest only after the passage into the plastic state. In this approach, additive rate of deformation decomposition is adopted when we use the symmetric part of the velocity gradient with respect to current position $\dot{\boldsymbol{\varepsilon}} = sym[\partial \mathbf{v} / \partial \mathbf{x}]$ and when the elastic strains are infinitesimal (negligible compared to unity):

$$\dot{\boldsymbol{\varepsilon}} = \dot{\boldsymbol{\varepsilon}}^{e} + \dot{\boldsymbol{\varepsilon}}^{p} + \dot{\boldsymbol{\varepsilon}}^{cr} \tag{1}$$

where $\dot{\boldsymbol{\varepsilon}}$ is the total strain rate, $\dot{\boldsymbol{\varepsilon}}^{e}$ is the elastic strain rate, $\dot{\boldsymbol{\varepsilon}}^{p}$ is the inelastic (plastic) time-independent strain rate, and $\dot{\boldsymbol{\varepsilon}}^{cr}$ is the inelastic (creep) time-dependent strain rate.

The elastic behavior can be modeled as linear elastic and the yield surface used with this model is written in terms of the two stress invariants:

- The equivalent pressure stress,

$$p = -\frac{1}{3} trace(\boldsymbol{\sigma}) \tag{2}$$

- The Von Mises equivalent stress,

$$\sigma_{eq} = \sqrt{\frac{3}{2}\mathbf{S}:\mathbf{S}} \tag{3}$$

where $\mathbf{S}$ is the stress deviator, defined as:

$$\mathbf{S} = \boldsymbol{\sigma} + p\mathbf{I} \tag{4}$$

and $\boldsymbol{\sigma}$ is the stress tensor.

The plasticity requires that the material satisfy a uniaxial-stress plastic-strain relationship. If the material is rate independent, the yield condition is written as:

$$\sigma_{eq} = \sigma_0 \tag{5}$$

where σ_0 is the yield stress.

If we also consider that, the material is rate dependent, and the uniaxial flow rate defined by the power-law model used in its "time hardening" form (Eq. (6)). This standard creep law is used for modeling secondary or steady-state creep. The power-law creep model is attractive for its simplicity. However, it is limited in its range of application. The time-hardening version of the power-law creep model is typically recommended only in cases when the stress state remains essentially constant.

$$\dot{\bar{\varepsilon}}^{cr} = A\sigma_{eq}^{n} t^{m} \tag{6}$$

where $\dot{\bar{\varepsilon}}^{cr}$ is the uniaxial equivalent creep strain rate defined as:

$$\dot{\bar{\varepsilon}}^{cr} = \sqrt{\frac{2}{3}\dot{\boldsymbol{\varepsilon}}^{cr} : \dot{\boldsymbol{\varepsilon}}^{cr}} \tag{7}$$

and t is the total time, and A, n, and m are model parameters. A and n must be positive and $-1 < m \leq 0$.
For the sake of simplicity of the approach, we consider the same elasto-viscoplastic material behavior at different scales (matrix constituents, homogenized matrix phase and HPC).

2.3 Microscale Modeling

At microscale level, it can be considered that the cementitious matrix is composed of four mechanically distinct phases [17], whose mechanical properties are accessible by nanoindentation. The principle of nanoindentation involves in applying a force with a very small diamond tip to the material surface and measuring simultaneously the corresponding penetration depth. By using this technique, different material properties, such as elastic modulus, hardness, plastic or viscous parameters, can be obtained from experimental results [42-44].
Considering that a 2-D axisymmetric simulation requires less computational time and is more convenient than a 3D model [45], a 2-D axisymmetric model was used for finite element simulation of the elasto-viscoplastic behavior of the four phases of the cementitious matrix in the nanoindentation process. A rigid conical indenter tip having a semi-spherical cap (which intersect at the unique location of common tangent) with a cone semi-apical angle of 70.3° was used in the axisymmetric model, which has the same projected area to depth function as the standard Berkovich indenter (Shim et al. 2004). Figure 2 shows the rigid indenter and the meshed specimen with 5329 four-node bilinear axisymmetric quadrilateral, reduced integration elements (CAX4R) of Abaqus Software [46]. A fine mesh was used under the contact area and near the tip of the indenter to define accurately the stress distribution under the indenter. Nonlinear geometry option was used in the finite element simulation. The sample height was considered about 50 times larger than the maximum indentation depth. Indentation was applied in the finite element simulations by load control as the experiment was with a linear loading in time followed by a holding period and an unloading phase. In the simulations, a contact interaction was applied by the definition of the indenter as 'master' and the sample as 'slave' surfaces. The coefficient of friction between the indenter tip and the specimen surface was set to 0.1 giving a better convergence of the contact algorithm, and it was verified that friction does not have a significant effect on the nanoindentation load–penetration depth response.

2.4 First Level Homogenization

After identification of elasto-viscoplastic properties of the constituent phases of the matrix, a finite element homogenization method was implemented to obtain the effective elasto-viscoplastic properties of the cementitious matrix. A two-dimensional numerical model is considered as a cross-section of a three-dimensional model with the same volume fraction.
To proceed with the analysis, we assume that the heterogeneous matrix is composed of four different phases (Fig. 3). The three phases and porosity are represented by ellipses and are randomly distributed in the fourth major phase. Fakhari Tehrani et al. [18] studied the influence of aggregate shape on the dynamic modulus values of asphalt mixes. They showed that inclusion shapes did not have a significant influence on the average of the corresponding complex modulus.
For the current study, a domain dimension of 100 μm × 100 μm is considered. To simulate a compression creep test, the domain is compressed between two rigid plates with frictionless conditions. The bottom plate is embedded and the top plate is submitted to a vertical constant or cyclic force for a creep period. The simulation is run under the plane stress conditions with time-dependent material response.

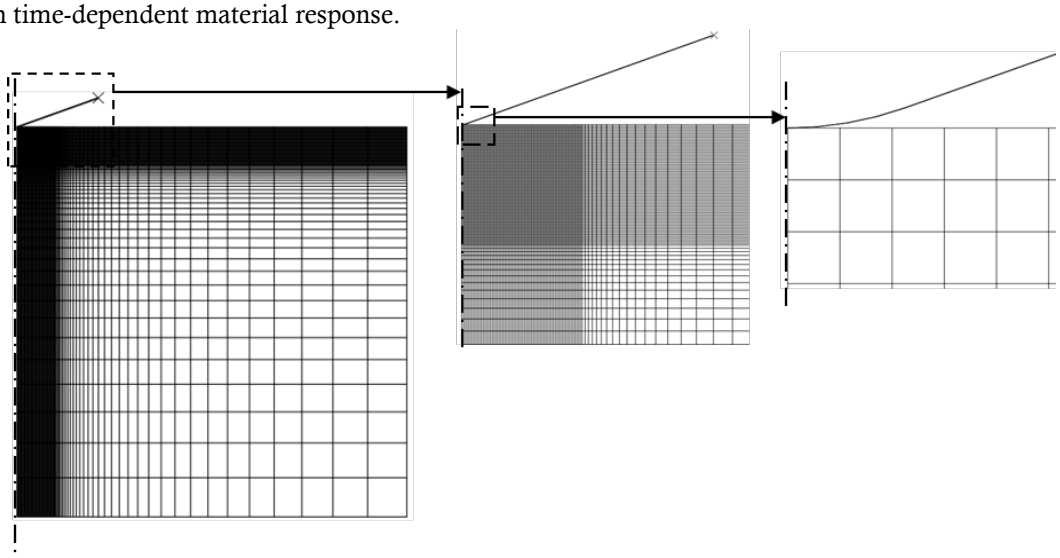

Fig. 2. Finite element mesh for the simulation of the axisymmetric nanoindentation problem.

Periodic boundary conditions (PBC) [47-48] are adopted on the limits of the RVE defined by the vertical walls of the domain such as:

$$u(x+L)-u(x)=\varepsilon^0 x, \qquad \forall x \in \Gamma_p \tag{8}$$

where u is the displacement at x, ε^0 is the strain applied to the RVE. Γ_p represents the boundary whose normal is along x direction. The PBC are applied through linear constraint equation in Abaqus [46].

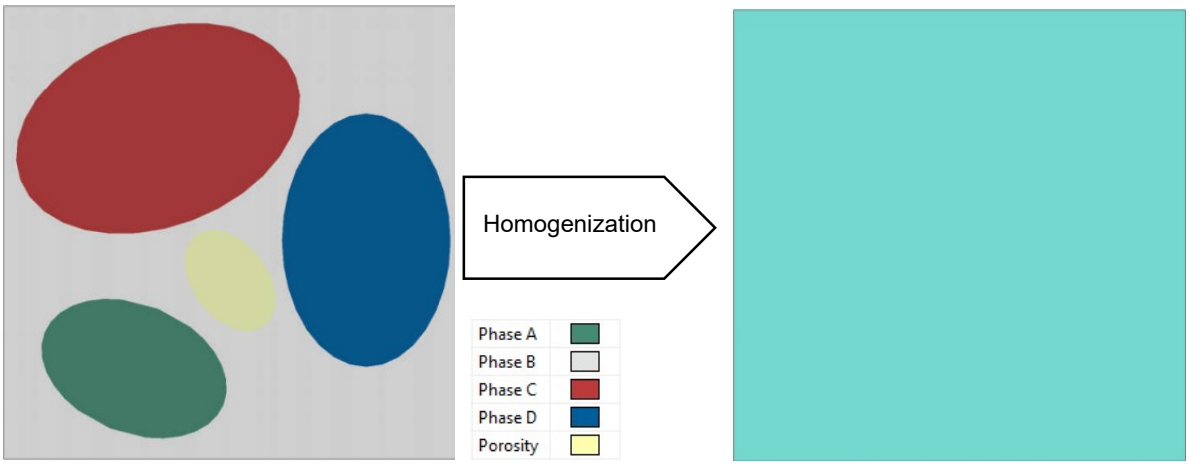

Fig. 3. First level homogenization.

To improve the accuracy of the results obtained, an investigation was performed to identify the optimal element size. Figure 4 shows the meshed heterogeneous and homogeneous domains with respectively 12139 and 625 four-node bilinear plane stress quadrilateral, reduced integration, with hourglass control elements (CPS4R) of Abaqus software [46].

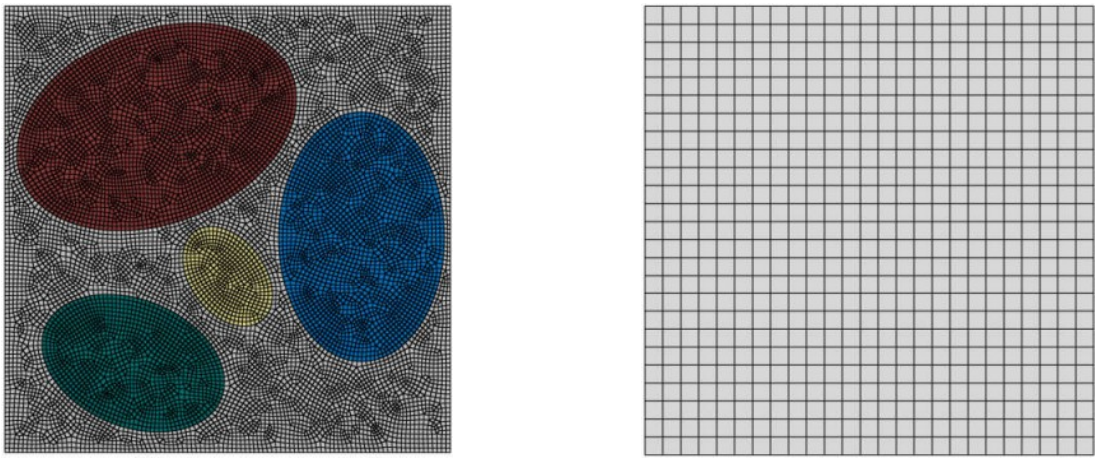

Fig. 4. Finite element meshes for heterogeneous and homogeneous matrix.

2.5 Second Level Homogenization

To access to the elasto-viscoplastic behavior of the whole mortar, a second level homogenization is needed. The composite material is constructed as the matrix (homogenized phase of the first level I) and the rest of components of the high performance such as aggregates, and capillary and large air pores. The interfacial zone (ITZ) between the matrix and the aggregate is not considered in this study.

The effective elasto-viscoplastic properties of the mortar are obtained by comparing the responses of homogeneous and heterogeneous mortar under the same creep conditions. As for the first level homogenization procedure, the error is computed as the root mean square of the differences between heterogeneous and homogeneous simulations over the entirety of the creep curve (Eq. (6)).

In this study, a domain dimension of 3.6 mm × 4.9 mm is considered. The finite element model of the meso-structure can be automatically obtained based on image of the realistic meso-structure which clearly represent aggregates, matrix material and voids respectively.

To simulate a compression creep test, the FE domain is compressed between two rigid plates with frictionless conditions. The bottom plate is embedded and the top plate is submitted to a vertical constant or cyclic force for a creep period. The simulation is run under the plane stress conditions with time-dependent material response. As for the first level

homogenization, periodic boundary conditions (PBC) are adopted on the limits of the domain defined by its vertical walls.

Before running the simulations, an investigation was performed to identify the optimal element size. Figure 5 shows the meshed heterogeneous and homogeneous domains with respectively 9620 and 2160 four-node bilinear plane stress quadrilateral, reduced integration, with hourglass control elements (CPS4R) of Abaqus software [46].

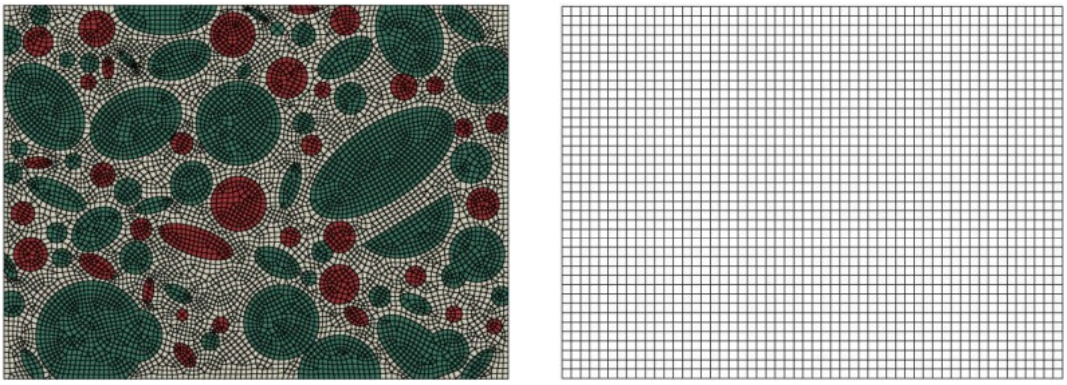

Fig. 5. Finite element meshes for heterogeneous and homogeneous concrete (Matrix: Gray, Aggregates: Green, Pores: Red).

3. Results and Discussion

To validate the method developed in the preceding paragraphs, we have used the experimental results from the work of Da Silva et al. [17]. They performed experimental tests on a high-performance composite at different levels of observation. They have also performed an analytical homogenization procedure to determine the elastic properties of the matrix and the whole mortar.

3.1 Identification of Elasto-viscoplastic Model for the Matrix Constituents from Nanoindentation Data

Da Silva *et al.* [17] have performed nanoindentation measurements on a cementitious matrix and have identified four mechanically distinct phases. For each phase, we have identified the parameters of the chosen elasto-viscoplastic constitutive model by matching the response of the numerical model with the experimental nanoindentation curves.

For each phase, the elastic modulus (E) was already determined by Da Silva *et al.* [17] using the Oliver–Pharr method [42] with the assumption of constant Poisson's ratio (ν=0.20).

However, the rate-dependent properties are not directly accessible by this technique. One way to determine such properties is the inverse method performed by combining finite element modelling and numerical optimization. In such method, the difference between experimental and numerical displacement-load curves is minimized with respect to the model parameters using numerical optimization and the parameters of the constitutive law are identified as the optimized solution [49-50].

In this work, the optimization process is driven by NSGA-II algorithm (Non-dominated Sorting Genetic Algorithm II) [51] which minimizes the error computed as the root mean square of the differences between simulation and experiment over the entirety of the indentation curve (loading and unloading):

$$f(\mathbf{P}) = \frac{1}{k}\sum_{i=1}^{k}\left(h_{sim}\left(\mathbf{P}, t_i\right) - h_{\exp}\left(t_i\right)\right)^2 \tag{9}$$

where $\mathbf{P} = \{\sigma_0, A, n, m\}$ is the vector of the unknown material parameters, k is the number of experimental data points, and h_{sim}, $h_{\exp}$ are the penetration depths of the simulated and experimental results respectively.

An initial random set of parameter vectors is generated. After achieving FE simulations using all the parameter vectors generated in the initial set, combinations of those providing the best results for the minimization of the objective function are used to generate a new set. This technique is repeated until having the parameter vector that provides the minimum difference between the numerical and experimental results.

Table 1 shows the identified model parameters obtained by the elasto-viscoplastic model for the four phases. The yield stress σ_0 has the lowest value for Phase A (66 MPa) composed of low stiffness porous phases and the greatest value for Phase D (350 MPa) containing the non-hydrated clinker and fly-ash. The parameter m is found to be close to -1 for Phase A, which demonstrates that this phase is more sensitive to creep due to the presence of porous phases. The parameters A and n are related to the yield stress and their effects are difficult to analyze separately.

Figure 6 presents the comparisons between the experimental data and numerical prediction using the parameters that are identified by the nanoindentation FE simulations for the four constitutive phases of the matrix. All comparisons indicate that there is a good agreement between the experimental measurements and the numerical simulations. The numerical simulations for nanoindentation experiments accurately predict the creep processes in the loading, holding and unloading stages. Therefore, it can be argued that the chosen constitutive model together with the identified parameters

from nanoindentation experiments can characterize the elasto-viscoplastic behavior of the different phases of the matrix. The numerical simulation results are closer to the experimental data in the unloading part than those in the loading and holding. This is because the unloading is purely elastic and the elastic moduli were directly identified from the experimental curves.

Table 1. The identified elasto-viscoplastic model parameters from nanoindentation tests.

	E (*) (GPa)	ν (*)	σ_0 (MPa)	A (MPa^{-n}.s$^{-(1+m)}$)	n	m
Phase A	19.6	0.2	66.0	$2.7\ 10^{-4}$	3.9	-0.96
Phase B	39.8	0.2	107.0	$5.0\ 10^{-6}$	2.1	-0.70
Phase C	50.9	0.2	300.0	$6.0\ 10^{-6}$	3.0	-0.75
Phase D	65.0	0.2	350.0	$1.0\ 10^{-6}$	2.0	-0.92

(*) From Da Silva *et al. [17]*.

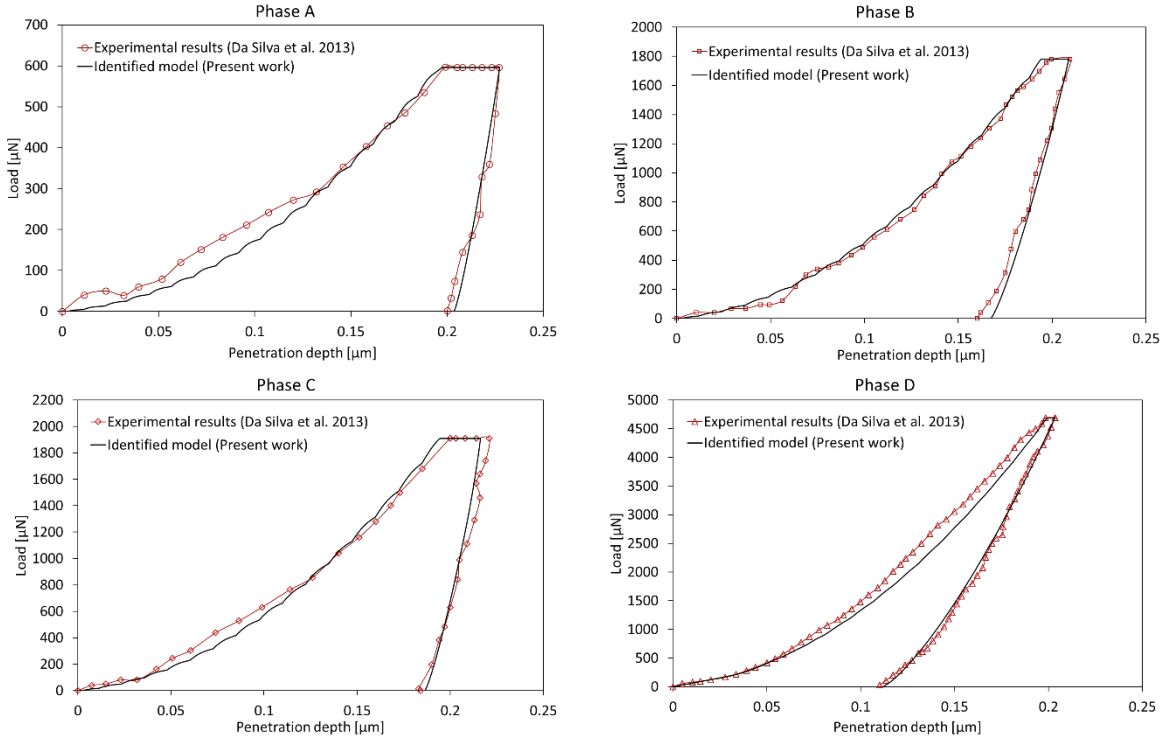

Fig. 6. Comparison between identified results using the elasto-viscoplastic model and the nanoindentation experimental results from Da Silva et al. [17].

3.2 Identification of first level homogenized elasto-viscoplastic model

Based on the identified elasto-viscoplastic model from nanoindentation tests of the matrix constituents, a finite element homogenization scheme was implemented. The heterogeneous matrix is composed of four different phases whose elasto-viscoplastic properties were identified in the precedent section. Phases A (9.5%), C (22.1%), D (16.3%) and the porosity (3.3%) are represented by ellipses and are randomly distributed in the fourth major phase B (48.9%).

The effective elasto-viscoplastic properties of the matrix are obtained by comparing the responses of homogeneous and heterogeneous matrices under the same compression conditions.

For the simulation of the compression test, the domain is compressed between two rigid plates with friction-free conditions. The bottom plate is fixed and the top plate is subjected to a vertical force. The simulation is carried out under the assumption of plane constraints. The periodic boundary conditions are imposed on the vertical walls of RVE. Since each of the phases of the cementitious matrix has its own elastic limit σ_0, we have introduced into the homogenized model a hardening modulus E_t to take into account the evolution of the elastic limit of the matrix.

We have used the same optimization process as for the matrix constituents. The error is computed as the root mean square of the differences between heterogeneous and homogeneous simulations over the compression curve.

The obtained results for the homogenized elasto-viscoplastic parameters for the matrix are presented in Table 2. The results show that the application of the numerical homogenization method resulted in effective elastic modulus very consistent with the results obtained by Da Silva *et al.* [17] with Mori-Tanaka analytical and FFT numerical schemes.

Figure 7 presents the comparison between FE simulations of the heterogeneous matrix and numerical predictions of homogeneous matrix using the identified elasto-viscoplastic model under compression conditions. The comparison indicates that there is a very good agreement between heterogeneous and homogeneous numerical simulations. The homogenized numerical model accurately predict the compression processes showing that the chosen constitutive model together with the homogenization procedure can simulate the elasto-viscoplastic behavior of the matrix.

Table 2. Identified elasto-viscoplastic model parameters from first level homogenization.

	E (GPa)	ν	σ_0 (MPa)	E_t (MPa)	A (MPa^{-n}.s$^{-(1+m)}$)	n	m
Present work	39.44	0.2	77.0	600.0	3.2 10^{-6}	2.2	-0.87
Mori-Tanaka scheme(*)	40.7	0.2	-	-	-	-	-
FFT scheme(*)	39.1-39.9	0.2	-	-	-	-	-

(*) From Da Silva *et al.* [17].

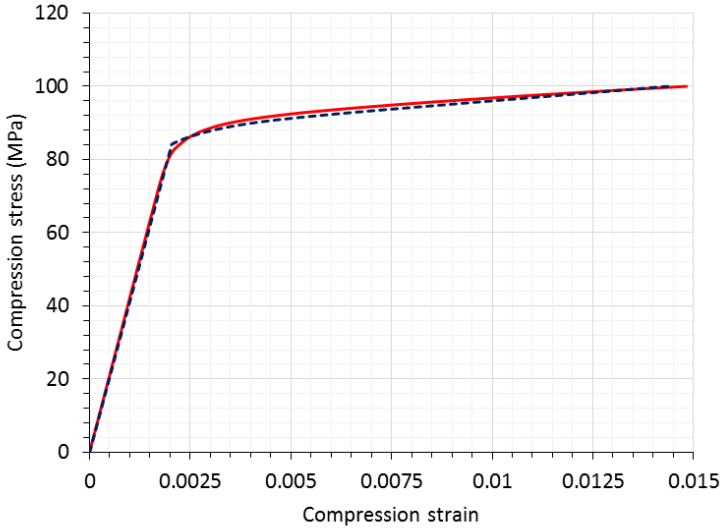

Fig. 7. Comparison between heterogeneous (continuous lines) and homogeneous (dashed lines) matrices under compression conditions.

3.3 Identification of second level homogenized elasto-viscoplastic model

To achieve level II homogenization corresponding to the HPC studied, we assume that it is composed of the already homogenized cement matrix (V_f = 46.3%), aggregates (V_f = 42.0%) and pores (broad and capillary, (V_f = 11.7%)). The porous structural configurations and physico-mechanical properties are seriously impacted by the geometrical shape of pores [52-55]. In the present work, the dimension of the RVE for the homogenization of the second level is 4.8 mm × 3.6 mm obtained from an image processing of a microscopic section of a HPC. The aggregates and pores are represented by circles or ellipses distributed in the cement matrix. As shown in Fig. 5, the heterogeneous HPC is idealized and a color code is adopted for each constituent as follows: the homogenized cement matrix is identified by gray, the aggregates by green and pores by red.

A convergence study of the mesh was carried out to identify the optimal size of the elements. Figure 5 shows the meshes of the heterogeneous RVE and the homogenized HPC using 9620 and 2160 four-node reduced integration quadrilateral elements (CPS4R) of the Abaqus software, respectively.

In the same way as for level I, the domain is compressed between two rigid plates with friction-free conditions. Table 3 resents the result of elasto-viscoplastic parameters for the HPC are presented obtained by our numerical homogenization model for level II compared to the results obtained by Da Silva *et al.* [17]. The elastic modulus we have obtained for the HPC is in very good agreement with the experimental elastic static and dynamic moduli. However, the effective elastic modulus calculated by Da Silva *et al.* [17] using the law of mixtures overestimates by an average of 14% the experimental modulus. The Poisson ratio (ν) and the compressive strength (σ_0) we have obtained for the HPC are also in a very good agreement with the values measured by Da Silva *et al.* [17].

Figures 8 and 9 present the comparison between FE simulations of the heterogeneous HPC and numerical predictions of homogeneous HPC using the identified elasto-viscoplastic model under compression and creep conditions respectively. The comparison indicates that there is a good agreement between heterogeneous and homogeneous numerical simulations. The homogenized numerical model accurately capture the compression and creep behaviors showing that the chosen constitutive model together with the homogenization procedure can simulate the elasto-viscoplastic behavior of HPC.

Table 3. Identified elasto-viscoplastic model parameters from the homogenized level II.

	E (GPa)	ν	σ_0 (MPa)	A (MPa^{-n}.s$^{-(1+m)}$)	n	m
Present work	35.0	0.18	44.8	1.2510^{-5}	1.86	-0.85
Mori-Tanaka scheme(*)	40.9	-	-	-	-	-
Static experiments(*)	34.9±1.54	-	47.4±4.23	-	-	-
Dynamic experiments(*)	36.7±1.27	0.19	-	-	-	-

(*) From Da Silva *et al.* [17].

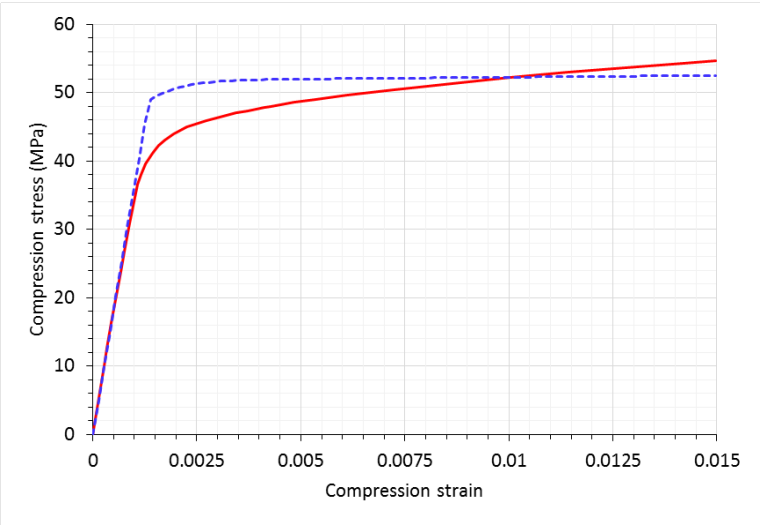

Fig. 8. Comparison between heterogeneous (continuous lines) and homogeneous (dashed lines) HPC under compression conditions.

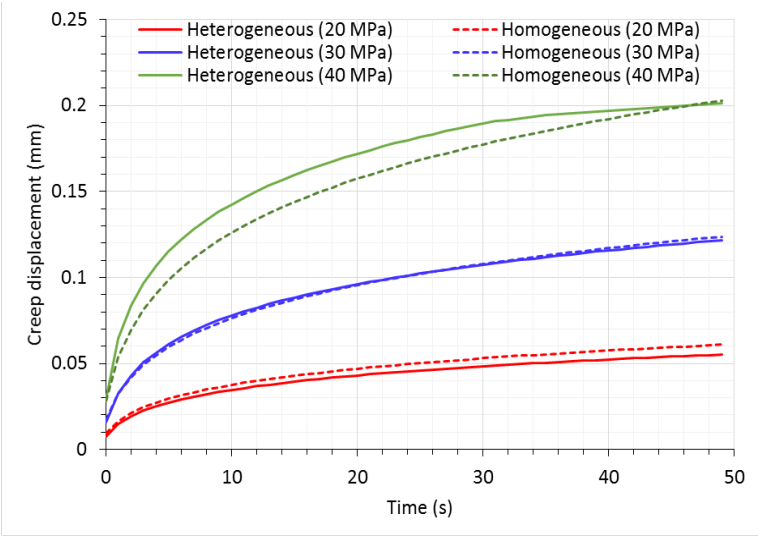

Fig. 9. Comparison between heterogeneous (continuous lines) and homogeneous (dashed lines) HPC under different creep conditions.

4. Conclusion

In this study, we developed an inverse identification methodology allowing the identification of the constitutive laws of the phases constituting the cement matrix of a HPC. The inverse identification method consists of comparing the finite element numerical simulations of the nanoindentation tests with the experimental results using a genetic algorithm to optimize the model parameters. The obtained results showed a good correlation between the experimental and numerical "load-depth of penetration" curves. After identifying the elasto-viscoplastic properties of the constituent phases of the cement matrix, a numerical homogenization method using the finite element method was implemented. This method firstly allowed to obtain the homogenized elasto-viscoplastic properties of the cement matrix and of the studied high-performance concrete. To achieve the homogenization of the first level corresponding to the cement matrix, we assumed that it consists of four mechanically distinct phases. The effective elastic modulus obtained by the numerical homogenization method was very consistent with the results obtained by Da Silva et al. [17] with the Mori-Tanaka analytical model and the FFT method. A very good agreement was found between the simulated compression stress vs compression strain curves for the heterogeneous RVE and homogenized cementitious matrix using the identified elasto-viscoplastic model. The proposed numerical homogenization model accurately predicted the equivalent elasto-viscoplastic behavior of the cement matrix. To achieve level II homogenization corresponding to the studied HPC, we assumed that it is composed of the already homogenized cement matrix, aggregates and pores (large and capillary). Aggregates and porosity were represented by ellipses distributed in the cement matrix. The effective elastic modulus, Poisson ration and compressive strength obtained by our Level II numerical homogenization procedure was in good agreement with the experimental results from the literature. A good agreement was also found between the simulated compression and creep curves for the heterogeneous RVE and homogenized HPC using the identified elasto-viscoplastic model.

Acknowledgment

This work was partially supported by the French HPC Center ROMEO.

Conflict of Interest

The authors declared no potential conflicts of interest with respect to the research, authorship and publication of this article.

Funding

The authors received no financial support for the research, authorship and publication of this article.

Nomenclature

A	Model parameter [MPa^{-n}.s$^{-(1+m)}$]	u	Displacement [μm]
E	Elastic modulus [GPa]	ε^0	Strain applied to the RVE
$f(\mathbf{P})$	Objective function	$\dot{\boldsymbol{\varepsilon}}$	Total strain rate
h_{exp}	Experimental penetration depth [μm]	$\dot{\boldsymbol{\varepsilon}}^e$	Elastic strain rate
h_{sim}	Computed penetration depth [μm]	$\dot{\boldsymbol{\varepsilon}}^p$	Inelastic (plastic) time-independent strain rate
m	Model parameter	$\dot{\boldsymbol{\varepsilon}}^{cr}$	Inelastic (creep) time-dependent strain rate
n	Model parameter	Γ_p	Boundary with normal along x direction
p	Equivalent pressure stress [MPa]	ν	Poisson coefficient
$\mathbf{P}$	Vector of the unknown material parameters	σ_0	Yield stress [MPa]
$\mathbf{S}$	Stress deviator tensor	σ_{eq}	Von Mises equivalent stress [MPa]
t	Total time [s]		

References

[1] Kanouté, P., Boso, D., Chaboche, J., Schrefler, B., Multiscale methods for composites: A review, *Archives of Computational Methods in Engineering*, 16, 2009, 31–75.
[2] Eshelby, J.D., The determination of the elastic field of an ellipsoidal inclusion, and related problems, *Proceedings of the Royal Society of London*, A241(1226), 1957, 376–396.
[3] Hill, R., The elastic behavior of a crystalline aggregate, *Proceedings of the Royal Society of London*, A65, 1952, 349–354.
[4] Hashin, Z., and Shtrikman, S., A variational approach to the elastic behavior of multiphase minerals, *Journal of the Mechanics and Physics of Solids*, 11(2), 1963, 127–140.
[5] Hershey, A., The elasticity of an isotropic aggregate of anisotropic cubic crystals, *Journal of Applied Mechanics – Transactions of the ASME*, 21(3), 1954, 236–240.
[6] Zohdi, T. I., Oden, J., Rodin, G. J., Hierarchical modeling of heterogeneous bodies, *Computer Methods in Applied Mechanics and Engineering*, 138(1-4), 1996, 273 – 298.
[7] Fish, J., Shek, K., Pandheeradi, M., Shephard, M. S., Computational plasticity for composite structures based on mathematical homogenization: Theory and practice, *Computer Methods in Applied Mechanics and Engineering*, 148(1-2), 1997, 53–73.
[8] Feyel, F., Multiscale FE2 elasto-viscoplastic analysis of composite structures, *Computational Materials Science*, 16(1-4), 1999, 344–354.
[9] Levy, A. and Papazian, J., Elastoplastic finite element analysis of short-fiber-reinforced SiC/Al composites: effects of thermal treatment, *Acta Metallurgica Materialia*, 39(10), 1991, 2255 – 2266.
[10] Ghosh, S., Lee, K. and Moorthy, S., Two scale analysis of heterogeneous elastic-plastic materials with asymptotic homogenization and voronoi cell finite element model, *Computer Methods in Applied Mechanics and Engineering*, 132(1-2), 1996, 63–116.
[11] Feyel, F. and Chaboche, J.-L., FE2 multiscale approach for modelling the elasto-viscoplastic behaviour of long fibre SiC/Ti composite materials, *Computer Methods in Applied Mechanics and Engineering*, 183(3-4), 2000, 309–330.
[12] Sun, L. and Ju, J., Effective elastoplastic behavior of metal matrix composites containing randomly located aligned spheroidal inhomogeneities. Part II: Applications, *International Journal of Solids and Structures*, 38(2), 2001, 203–225.
[13] Borges, D.C. and Pituba J.J.C., Analysis of quasi-brittle materials at mesoscopic level using homogenization model, *Advances in Concrete Construction*, 5(3), 2017, 221-240.
[14] Constantinides, G. and Ulm, F.J., The effect of two types of C–S–H on the elasticity of cement-based materials: results from nanoindentation and micromechanical modeling, *Cement and Concrete Research*, 34(1), 2004, 67–80.

[15] Sorelli, L., Constantinides, G., Ulm, F.J. and Toutlemonde, F., The nano-mechanical signature of ultra-high performance concrete by statistical nanoindentation techniques, *Cement Concrete Research*, 38(12), 2008, 1447–1456.
[16] Němeček, J., Králík, V. and Vondrejc, J., Micromechanical analysis of heterogeneous structural materials, *Cement and Concrete Composites*, 36, 2013, 85–92.
[17] Da Silva, W.R.L., Němeček, J. and Štemberk, P., Application of multiscale elastic homogenization based on nanoindentation for high performance concrete, *Advances in Engineering Software*, 62–63, 2013, 109–118.
[18] Fakhari Tehrani, F., Absi, J., Allou, F. and Petit, Ch., Heterogeneous numerical modeling of asphalt concrete through use of a biphasic approach: Porous matrix/inclusions, *Computational Materials Science*, 69, 2013, 186–196.
[19] Zhou, C., Li, K. and Ma, F., Numerical and statistical analysis of elastic modulus of concrete as a three-phase heterogeneous composite, *Computers and Structures*, 139, 2014, 33–42.
[20] Caballero, A., Lopez, C.M. and Carol, I., 3D meso-structural analysis of concrete specimens, *Computer Methods in Applied Mechanics and Engineering*, 195, 2006, 7182–7195.
[21] Shahbeyk, S., Hosseini, M. and Yaghoobi, M., Mesoscale finite element prediction of concrete failure, *Computational Materials Science*, 50, 2011, 1973–1990.
Shim, S., Oliver, W.C. and Pharr, G.M., A critical examination of the Berkovich vs. conical indentation based on 3D finite element calculation, *MRS Proceedings*, 841, 2004, R9.5.
[22] Sun, B. and Li, Z., Adaptive concurrent multi-scale FEM for trans-scale damage evolution in heterogeneous concrete, *Computational Materials Science*, 99, 2015, 262–273.
[23] Tedesco, J.W., Hughes, M.L. and Ross, C.A., Numerical simulation of high strain rate concrete compression tests, *Computers & Structures*, 51(1), 1994, 65–77.
[24] Tedesco, J.W., Powell, J.C., Ross, C.A. and Hughes, M.L., A strain-rate-dependent concrete material model for ADINA, *Computers & Structures*, 64(5-6), 1997, 1053–1067.
[25] Beshara, F. and Virdi, K., Prediction of dynamic response of blast-loaded reinforced concrete structures, *Computers & Structures*, 44(1-2), 1992, 297–313.
[26] Cela, J.J.L., Analysis of reinforced concrete structures subjected to dynamic loads with a viscoplastic Drucker–Prager model, *Applied Mathematical Modelling*, 22(7), 1998, 495–515.
[27] Shirai, K., Ito, C. and Onuma, H., Numerical studies of impact on reinforced concrete beam of hard missile, *Nuclear Engineering and Design*, 150, 1994, 483–489.
[28] Park, S.W., Xia, Q. and Zhou, M., Dynamic behavior of concrete at high strain rates and pressures: II. Numerical simulation, *International Journal of Impact Engineering*, 25, 2001, 887–910.
[29] Buck, J. J., McDowell, D.L. and Zhou, M., Effect of microstructure on load-carrying and energy-dissipation capacities of UHPC, *Cement and Concrete Research*, 43, 2013, 34-50.
[30] Häfner, S., Eckardt, S., Luther, T. and Könke, C., Mesoscale modeling of concrete: Geometry and numerics, *Computers & Structures*, 84(7), 2006, 450–461.
[31] Dupray, F., Malecot, Y., Daudeville and L., Buzaud, E., A mesoscopic model for the behaviour of concrete under high confinement, *International Journal for Numerical and Analytical Methods in Geomechanics*, 33(11), 2009, 1407–1423.
[32] Comby-Peyrot, I., Bernard, F., Bouchard, P., Bay, F. and Garcia-Diaz, E., Development and validation of a 3D computational tool to describe concrete behaviour at mesoscale. Application to the alkali-silica reaction, *Computational Materials Science*, 46, 2009, 1163–1177.
[33] Aydin, A.C., Arslan, A. and Gül, R., Mesoscale simulation of cement based materials' time-dependent behavior, *Computational Materials Science*, 41, 2007, 20–26.
[34] Setiawan, Y., Gan, B.S. and Han, A.L., Modeling of the ITZ zone in concrete: Experiment and numerical simulation, *Computers and Concrete*, 19(6), 2017, 647-655.
[35] Xu, W., Wu, F., Jiao, Y., Liu, M., A general micromechanical framework of effective moduli for the design of nonspherical nano- and micro-particle reinforced composites with interface properties, *Materials & Design*, 127, 2017, 162–172.
[36] Xu, W., Jia, M., Zhu, Z., Liu, M., Lei, D., Gou, X., n-Phase micromechanical framework for the conductivity and elastic modulus of particulate composites: Design to microencapsulated phase change materials (MPCMs)-cementitious composites, *Materials & Design*, 145, 2018, 108–115.
[37] Xu, W., Wu, Y., Gou, X., Effective elastic moduli of nonspherical particle-reinforced composites with inhomogeneous interphase considering graded evolutions of elastic modulus and porosity, *Computer Methods in Applied Mechanics and Engineering*, 350, 2019, 535–553.
[38] Xu, W., Zhang, D., Lan, P., Jiao, Y., Multiple-inclusion model for the transport properties of porous composites considering coupled effects of pores and interphase around spheroidal particles, *International Journal of Mechanical Sciences*, 150, 2019, 610–616.
[39] Xu, W., Xu, B., Guo, F., Elastic properties of particle-reinforced composites containing nonspherical particles of high packing density and interphase: DEM–FEM simulation and micromechanical theory, *Computer Methods in Applied Mechanics and Engineering*, 326, 2017, 122–143.
[40] Xu, W., Sun, H., Chen, W., Chen, H., Transport properties of concrete-like granular materials interacted by their microstructures and particle components, *International Journal of Modern Physics B*, 32(18), 2018, 1840011.
[41] Perzyna, P., Fundamental problems in viscoplasticity, *Advances in Applied Mechanics*, 9, 1966, 243–377.
[42] Oliver, W.C and Pharr, G.M., An improved technique for determining hardness and elastic modulus using load and

displacement sensing indentation experiments, *Journal of Material Research*, 7(6), 1992, 1564–1583.
[43] Guessasma, S., Sehaki, M., Lourdin, D. and Bourmaud, A., Viscoelasticity properties of biopolymer composite materials determined using finite element calculation and nanoindentation, *Computational Materials Science*, 44, 2008, 371–377.
[44] Chen, Z., Diebels, S., Peter, N.J. and Schneider, A.S., Identification of finite viscoelasticity and adhesion effects in nanoindentation of a soft polymer by inverse method, *Computational Materials Science*, 72, 2013, 127–139.
[45] Benkabou, R., Abbès, B., Abbès, F., Asroun, A. and Li, Y. (), Contribution of 3D numerical simulation of instrumented indentation testing in the identification of elastic-viscoplastic behaviour law of a high-performance concrete, *Matériaux & Techniques*, 105, 2017, 102.
[46] Abaqus Version 6.13, Dassault Systèmes Simulia Corp., Providence, RI, USA, 2013.
[47] Wang, X.F., Wang, X.W., Zhou, G.M. and Zhou, C.Z., Multi-scale analysis of 3D woven composite based on periodicity boundary conditions, *Journal of Composite Materials*, 41(14), 2007, 1773-1788.
[48] Melro, A.R., Camanho, P.P., Andrade Pires, F.M. and Pinho, S.T., Micromechanical analysis of polymer composites reinforced by unidirectional fibres: Part II – Micromechanical analyses, *International Journal of Solids and Structures*, 50(11-12), 2013, 1906–1915.
[49] Bocciarelli, M., Bolzon, G. and Maier, G., Parameter identification in anisotropic elastoplasticity by indentation and imprint mapping, *Mechanics of Materials*, 37, 2005, 855–868.
[50] Nakamura, T. and Gu, Y., Identification of elastic-plastic anisotropic parameters using instrumented indentation and inverse analysis, *Mechanics of Materials*, 39, 2007, 340–356.
[51] Deb, K., Pratap, A., Agarwal, S. and Meyarivan, T., A fast and elitist multiobjective genetic algorithm: NSGA-II, *IEEE Transactions on Evolutionary Computation*, 6(2), 2002, 182–197.
[52] Trofimov, A., Abaimov, S. G., Akhatov, I., Sevostianov, I., On the bounds of applicability of two-step homogenization technique for porous materials, *International Journal of Engineering Science*, 123, 2018, 117–126.
[53] Trofimov, A., Markov, A., Abaimov, S. G., Akhatov, I., Sevostianov, I., Overall elastic properties of a material containing inhomogeneities of concave shape, *International Journal of Engineering Science*, 132, 2018, 30–44.
[54] Xu, W., Jia, M., Gong, Z., Thermal conductivity and tortuosity of porous composites considering percolation of porous network: From spherical to polyhedral pores, *Composites Science and Technology*, 167, 2018, 134–140.
[55] Xu, W., Jiao, Y., Theoretical framework for percolation threshold, tortuosity and transport properties of porous materials containing 3D non-spherical pores, *International Journal of Engineering Science*, 134, 2019, 31–46.

ORCID iD

Fazilay Abbès https://orcid.org/0000-0003-0036-822X
Boussad Abbès https://orcid.org/0000-0003-1192-6549

© 2020 by the authors. Licensee SCU, Ahvaz, Iran. This article is an open access article distributed under the terms and conditions of the Creative Commons Attribution-NonCommercial 4.0 International (CC BY-NC 4.0 license) (http://creativecommons.org/licenses/by-nc/4.0/).